Metabolic profiling, histopathological anti-ulcer study, molecular docking and molecular dynamics of ursolic acid isolated from *Ocimum forskolei* Benth. (family *Lamiaceae*)

Eman Maher Zahran[a,*], Usama Ramadan Abdelmohsen[a,b], Ahmed Taha Ayoub[c], M. Alaraby Salem[d], Hany Ezzat Khalil[e], Samar Yehia Desoukey[b], Mostafa Ahmed Fouad[b], Mohamed Salah Kamel[b]

[a] *Department of Pharmacognosy, Faculty of Pharmacy, Deraya University, Universities Zone, 61111 New Minia City, Egypt*
[b] *Department of Pharmacognosy, Faculty of Pharmacy, Minia University, 61519 Minia, Egypt*
[c] *Department of Medicinal Chemistry, Heliopolis University, 3 Cairo-Belbeis Desert Road, El-Nahda, Qism El-Salam, Cairo 11777, Egypt*
[d] *Department of Pharmaceutical Chemistry, Faculty of Pharmacy, October University of Modern Sciences and Arts (MSA), Giza, Egypt*
[e] *Department of Pharmaceutical Sciences, College of Clinical Pharmacy, King Faisal University, 31982 Al-Ahsa, Saudi Arabia*

ARTICLE INFO

ABSTRACT

Ocimum forskolei (Habak), *Lamiaceae*, is an endemic species from Yemen and KSA; where our present study was aimed at investigating the Metabolic profiling coupled with LC−HR-MS analysis of the dichloromethane fraction from the aerial parts of that plant with a special emphasis on ursolic acid as the major predominating compound from this fraction. Histopathological evaluation of ursolic acid in different doses against indomethacin-induced ulcers in rats revealed a highly significant and dose dependent protection. With the dose level of 50 mg/kg b.w., Ursolic acid gave an ulcer index of 1.33 ± 0.33 and 97.8% inhibition, compared to cimetidine as a standard with 3.0 ± 0.58 and 95.2%. To rationalize this activity, docking on various macromolecular targets was performed, followed by molecular dynamics on the most promising target; the M3 receptor. A high binding energy of -344 kJ/mol is predicted between Ursolic acid and the protein indicating the stability of the predicted pose.

© 2020 SAAB. Published by Elsevier B.V. All rights reserved.

1. Introduction

Peptic ulcer is one of the most prevalent gastrointestinal disorders in the world affecting approximately 5−10% of people during their life and one of their most prevalence causes are the nonsteroidal anti-inflammatory drugs (NSAIDs) such as Indomethacin (Sumbul et al., 2011). The need for development of a suitable and effective antiulcer drug from a natural; plant-derived source; devoiding of side effects is one of the major scientific challenges across the globe. Many plants with triterpenoidal compounds excert anti-ulcer and gastroprotective effects (Arrieta, 2003), and this was the lead for us to examine *Ocimum forskolei* Benth., tha aromatic lamiaceous herb

belonging to the genus *Ocimum* which rich with a diversity of such compounds (Singh and Chaudhuri, 2018). *O. forskolei* is native to East Africa from Egypt, south to Kenya, and in Asia from Yemen to Oman, and the UAE (Fatope et al., 2008) and it was traditionally used as a mosquito repellent in Eritrea and antiflu in UAE (Dekker et al., 2011; Ali et al., 2017). The plant essential oil exhibited antioxidant, antimicrobial and cytotoxic activities (Ali et al., 2017) but no effort has been done to evaluate the antiulcer potential of its individual compounds. In this context, the aim of the present study was to investigate the antiulcer potential of ursolic acid (UA) which is the most prevalent compound in *O. forskolei* and the most abundant constituent detected in the genus *Ocimum* giving a 0.252−0.478% w/w and 0.62−19.10 mg/g existence by many quantification studies using HPTLC and UPLC-ESI−MS/MS techniques, respectively (Prabhu et al., 2009). The study also aimed at further confirmation of the results with both molecular docking analysis and molecular dynamic simulation study. UA is a lipophilic pentacyclic triterpene (Lee et al., 2016), having a diverse bioactivities such as: anti-inflammatory (Baricevic et al., 2001), antitumor (Yang et al., 2015), anti-apoptotic (Kim and

Moon, 2015), antihepatotoxic (Ma et al., 2015), anti-HIV (Kashiwada et al., 2000), and antituberculosis (Cantrell et al., 2001).

2. Materials and methods

2.1. Collection of plant and sample preparation

Aerial parts (leaves and stems) of *O. forskolei* (8 kg) were collected in September 2016 from the National Garden of Jazan, KSA. The plant specimen was identified by Dr. Mahmoud Abdelhady Hassan, Professor of Horticulture, Faculty of Agriculture, Minia University. A voucher specimen (Mn-ph-Cog-038) was kept in the herbarium of Pharmacognosy Department, Faculty of Pharmacy, Minia university, Minia, Egypt.

Samples from the air dried aerial parts of *O.forskolei* were extracted by maceration with 95% ethanol. The total ethanol extract (TEE; 400 g) was suspended in a small amount of water to give the aqueous solution which was successively partitioned in a large separating funnel with various organic solvents: petroleum ether (pt. ether), dichloromethane (DCM), and ethyl acetate (EtOAc). The organic phase was then concentrated to give the different fractions: Pt. Ether (120 g), DCM (35 g) and EtOAc (32), and the remaining mother liquor was then concentrated to give the aqueous fraction and all the resulted fractions were kept at 4 °C for further studies.

2.2. LC—HR-MS analysis

Acquity Ultra Performance Liquid Chromatography system coupled to a Synapt G2 HDMS quadrupole time-of-flight hybrid mass spectrometer (Waters, Milford, USA). Chromatographic separation was carried out on a BEH C18 column (2.1 × 100 mm, 1.7 μm particle size; Waters, Milford, USA) with a guard column (2.1 × 5 mm, 1.7 μm particle size) and a linear binary solvent gradient of 0%−100% eluent B over 6 min at a flow rate of 0.3 mL min^{-1}, using 0.1% formic acid in water (v/v) as solvent A and acetonitrile as solvent B. The injection volume was 2 μL and the column temperature was 40 °C. To convert the raw data into separate positive and negative ionization files, Ms converter software was used Using MZmine 2.12 as framework for MS data differential analysis were, the raw data were imported by selecting the ProteoWizard−converted positive or negative files in mzML format (Tawfike et al., 2019) (Ibrahim et al., 2018). (DNP and METLIN databases were used for dereplicating each *m/z* ion peak (using RT and *m/z* threshold of ±5 ppm), which provided the putative identities of all metabolomes in the total extract (s) in details (Elsayed et al., 2018).

2.2.1. Phytochemical study

A part of fraction II (15 g) was subjected to VLC fractionation on a silica gel column. Elution was performed using Pet. ether-EtOAc gradient mixtures in the order of increasing polarities (20, 30, 40, 50 and 100%). The effluents were collected in fractions (100 ml each); each fraction was concentrated and monitored by TLC. Similar fractions were grouped together and concentrated under reduced pressure to provide five subfractions (II 1-II 5). Subfraction II 4 (3 g) was fractionated over silica gel column using DCM-MeOH gradient mixtures to yield three subfractions (II 4, 1−3) and a white precipitate was heavily formed in the three subfractions. It was purified and washed several times with pet. ether to remove chlorophyll and other impurities. The precipitated compound was subjected to ^{1}H NMR analysis followed by co-chromatography in comparison with an authentic ursolic acid sample obtained from pharmacognosy department, faculty of pharmacy, Minia university. The run system used for TLC co-chromatography was DCM:Methanol 95:5 and the R$_f$ value was measured.

2.3. ADME-toxicity

The ADME-toxicity for the compound was predicted using the online platform of SwissADME (Daina et al., 2017). The summary of data is provided in Table S1.

2.4. Animals

Thirty healthy a dult male albino rats were used randomized into 6 groups of 5 rats each (150 ± 50 g each) in compliance with the guidelines for the care and use of laboratory animals of the National Institutes of Health (Giles 1987). Rats were housed under standardized conditions of temperature (23 ± 2 °C) and humidity (55 ± 15%) in the pre-clinical animal house and were deprived of food 24 h before the experiment to ensure an empty stomach; but allowed free access to water; and kept in mesh-bottomed cages to minimize coprophagia. Acclimatization for the experiment was done for one week before commencement of the experiment and all conditions were made to minimize animal suffering. All rats were employed in the experiment at the same time of the day to avoid variations due to diurnal rhythms of putative regulators of gastric functions (Ozbakiş and Gürsan, 2005).

2.5. Subacute toxicity study

The toxicity of the extract was assessed as previously described (Schapoval et al., 1998) by measuring the lethal dose for 50% of the laboratory animals (LD$_{50}$ method). Healthy rats were categorized into three groups, orally given UA at the doses of 500, 1000, 1500 mg/kg b. w. (suspended in 0.5% CMC as vehicle) and observed for 48 h under normal environmental conditions, with free access to food and water.

2.6. In vivo antiulcer study

Different concentrations (50, 100 and 150 mg/kg b.w.) of ursolic acid were evaluated for their anti-ulcer activity using the indomethacin-induced gastric ulcer model in rats (Batista et al., 2004; Ozbakiş and Gürsan, 2005; Arun and Asha, 2008). The experimental animals were randomly divided into six groups of five rats each. Treatments were given orally and carried out according to the following allotment: Group 1 served as the normal control group, which received the vehicle (0.5% CMC) only. Group 2 served as the positive control group and was given cimetidine (100 mg/kg). Group 3 served as the negative control group, received the vehicle (0.5% CMC). Groups 4−6 were administered the tested concentrations 50, 100 and 150 mg/kg p.o. (dissolved in 0.5% CMC solution). After one hour, groups 2−6 received the indomethacin dose (40 mg/kg, p.o.) to induce gastric ulcers, and five hours later, all rats were sacrificed by cervical dislocation. The stomachs were removed, incised along their greater curvature, washed delicately with tap water then with normal saline to remove gastric contents, examined for macroscopical mucosal lesions and then prepared for histopathological examination (Arun and Asha, 2008) by both light and scanning electron microscopes.

2.6.1. Assessment of gastric mucosal lesions

The ulcer index (UI) is calculated by examination of the stomachs with the aid of an eye piece using a 0−3 scoring system. The severity factor is calculated as: level 0 = no lesions; level 1 = lesions < 1 mm length, level 2 = lesions 2−4 mm length and level 3 = lesions > 4 mm length. The lesions score for each rat was calculated as the number of lesions multiplied by their respective severity factor (Table 2, Figs. 4, 5 and S5). The preventive index (PI) was calculated by the following equation (Inas et al., 2011):

$$PI = \frac{[UI\ of\ indomethacin\ group] - [UI\ for\ the\ treated\ group]}{[UI\ of\ indomethacin\ group]} \times 100$$
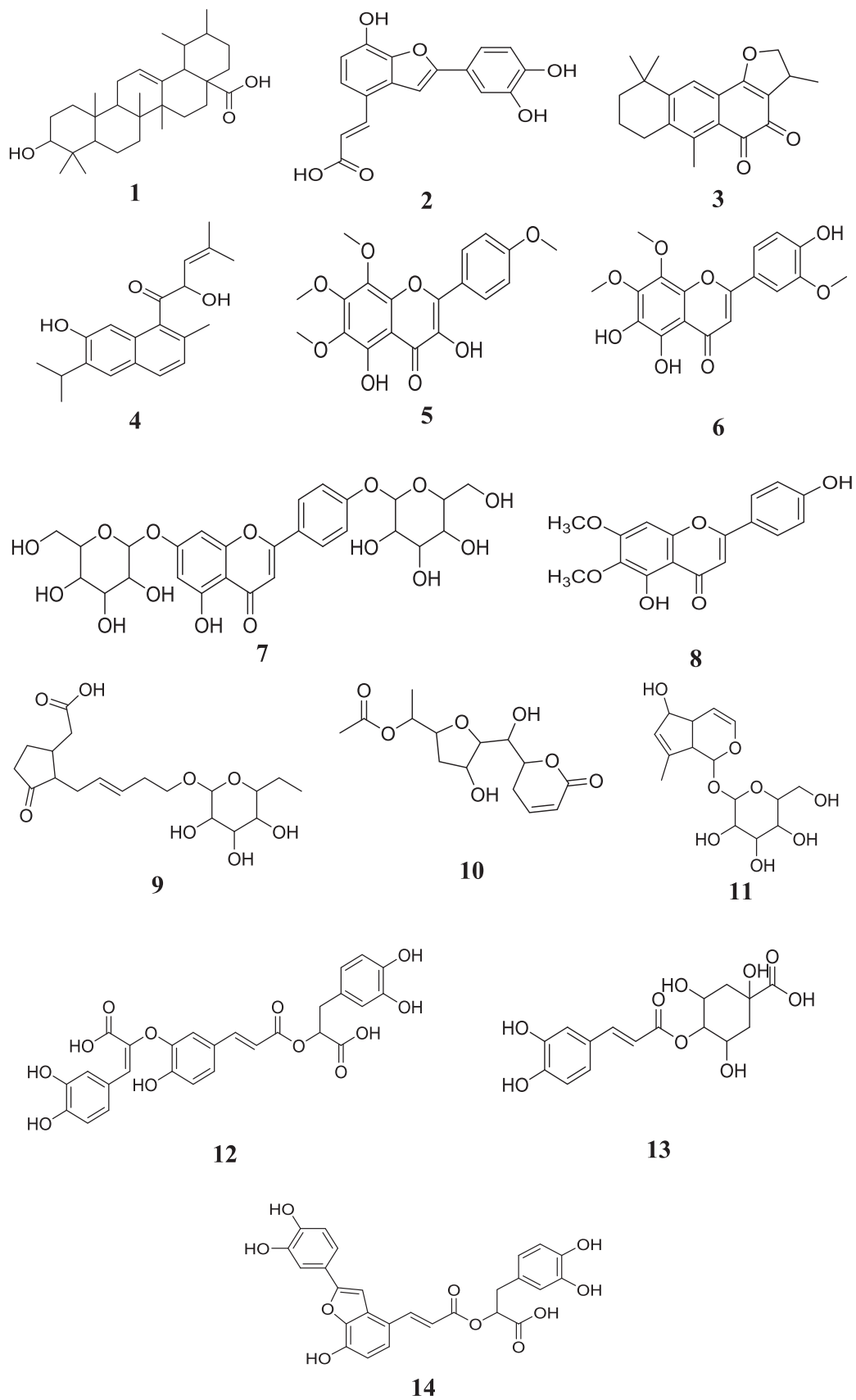
Fig. 1. Chemical composition of dereplicated compounds by metabolic analysis from DCM fraction of *O. forskolei*. (Full names of these compounds are found in table 1).

Table 1
Identification of chemical composition of different metabolites from DCM fraction of *O. forskolei*.

No	Compound	*m/z*	Hit rate/Similarity indec ratio (%)	R_t	M.f.	M.wt.(g/mol)
1	Ursolic acid	456.364	98.9%	3.571	$C_{30}H_{48}O_3$	456.711
2	Tournefolic acid Polyphenol	313.067	94.0%	4.110	$C_{17}H_{12}O_6$	312.062
3	Aegyptinone A Diterpene quinone	310.158	99.1%	4.841	$C_{20}H_{22}O_3$	310.157
4	Limbinol Abietane diterpene	312.176	98.7%	312.18	$C_{20}H_{24}O_3$	312.41
5	3,5-Dihydroxy-4′,6,7,8-tetramethoxyflavone Flavonoid	374.103	97.1%	3.562	$C_{19}H_{18}O_8$	374.099
6	4′,5,6-Trihydroxy-3′,7,8-trimethoxy-flavone (thymonin) Flavonoid	360.088	96.6%	2.944	$C_{18}H_{16}O_8$	360.083
7	Apigenin-7,4′-di-O-glucoside Flavonoid glycoside	594.162	97.5%	2.632	$C_{27}H_{30}O_{15}$	594.158
8	5,4′-dihydroxy-6,7-dimethoxyflavone (Cirsimaritin)	314.079	100%	4.22	$C_{17}H_{14}O_6$	314.078
9	Jasmonic acid; 12-Hydroxy, O-β-D-glucopyranosideAlkyl cyclopentanone	386.197	98.5%	2.508	$C_{18}H_{28}O_9$	388.17
10	Synparvolide C Cyclopentanone	300.124	97.5%	2.289	$C_{14}H_{20}O_7$	300.12
11	Linaride Iridoid	330.135	97.8%	2.476	$C_{15}H_{22}O_8$	330.131
12	Isomelitric acid A Polyphenol	538.114	97.4%	3.023	$C_{27}H_{22}O_{12}$	538.112
13	4-O- Caffeoylquinic acid (Caffeic derivative)	354.093	98.8%	2.256	$C_{16}H_{18}O_9$	354.095
14	Salvianolic acid C Caffeic acid derivative	493.112	99.2%	3.338	$C_{26}H_{20}O_{10}$	492.105
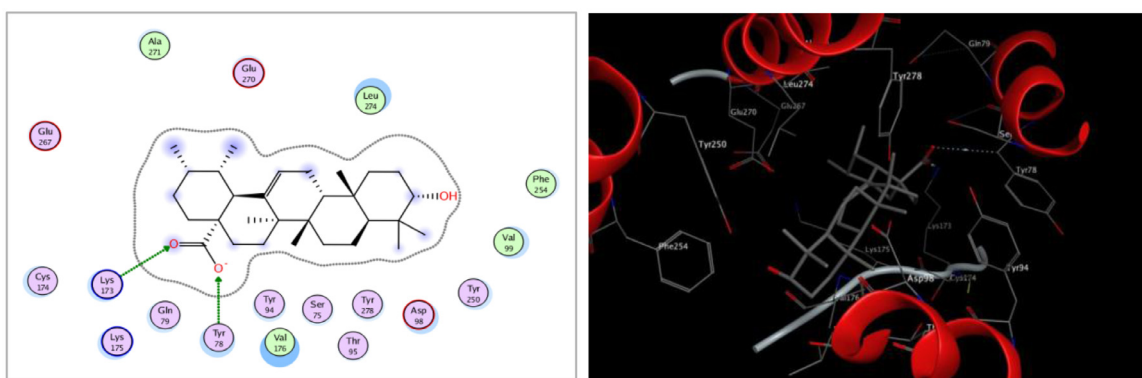
Fig. 2. 2D and 3D docking interaction diagrams of ursolic acid with the H2 receptor *via* the carboxylic function group.
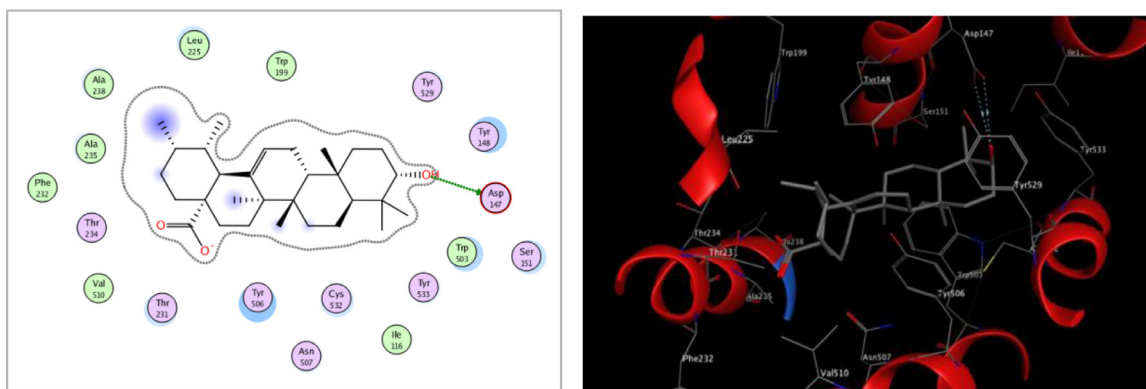
Fig. 3. 2D and 3D docking interaction diagrams of ursolic acid with the M3 receptor *via* the hydroxylic function group.

Table 2
Antiulcer activity of different concentrations of UA.

Group	Level 1 (mm)	Level II (mm)	Level III (mm)	UI (mm)	PI (%)
Indomethacin + cimetidine (+ve control)	2.33 ± 0.33	0.3 ± 0.33	0	3 ± 0.58	95.2
1 Indomethacin (-v control)	16.33 ± 1.2	12.67 ± 2.96	8.33 ± 1.86	62 ± 13.11	–
Group A (50 mg/kg)	1.33 ± 0.33	0	0	1.33 ± 0.33	97.8
Group B (100 mg/kg)	1.33 ± 0.33	1.33 ± 0.33	0	4 ± 0.58	93.5
Group C (150 mg/kg)	6.33 ± 0.88	3.33 ± 0.88	1 ± 0.58	15.33 ± 3.18	72.3

2.6.2. Histopathological preparations for LEM and SEM examination

2.6.2.1. Light electron microscopic examination (LEM). A longitudinal section of the gastric tissue was taken from the glandular part of the stomach of each rat and fixed in a 10% buffered formalin solution, embedded in paraffin, and then sectioned at 4−5 μm using a microtome. After removal of paraffin, the prepared sections were stained with alum-hematoxylin and eosin and evaluated microscopically for histopathological changes (Inas et al., 2011). Finally, their images were captured using a LEICA, DM1000 microscope with a digital camera (LEICA, EC3, Germany).

2.6.2.2. Scanning electron microscopic examination (SEM). One gastric tissue block was excised from different rats of each group, rinsed with cocodylate buffer and placed in 2.5% glutaraldehyde. Following fixation, the specimens were washed several times with cold cocodylate buffer and post-fixed in 1% osmium tetraoxide. They were dehydrated in a graded ethanol series, exposed to liquid CO_2 in a critical point drying apparatus and then coated with a thin layer of gold (10−15 um) deposited over the surface in a vacuum evaporator, then they were ready for microscopical examination (Nanjundaiah et al., 2011).

2.6.3. Statistical analysis

Data were expressed as mean $\pm$ standard error of mean (S.E.M) (n = 5). One-way analysis of variance (ANOVA) followed by Dunnett's test was applied. Graph Pad Prism 5 was used for statistical calculations (Graph pad Software, San Diego, California, USA). Results were regarded as significant as follows: *$P < 0.05$, **$P < 0.01$, ***$P < 0.001$.

2.7. Molecular docking analysis

Four macromolecular structures that are involved in gastric acid secretion were used to study the anti-ulcer activity of the compounds (Baba, 2018). The first is the M3 muscarinic acetylcholine receptor whose structure has been elucidated *via* crystallography and deposited in the protein databank with ID of 5ZHP. In addition, the compounds were docked against the gastrin and histamine targets in the parietal cells, CCK2 and H2-receptor, respectively. CCK2 and H2 receptors belong to the GPCR family and their structures have not been solved, so homology models from the GPCR database were used. The fourth structure used in the experiment is the proton pump crystal structure with ID 5YLU. Cimetidine was also docked as the positive control drug for the experiment (Table S2). A grid box of dimensions 50 grid points and spacing 0.375 was centered on the given co-crystallized ligand in the case of M3-receptor and the proton pump. For CCK2 and H2, the active sites were determined by homology to similar proteins with co-crystallized ligands. Four conformations were generated for each ligand using OpenBabel (Babel, 2011), and docking was performed *via* Autodock4 (Morris et al., 2009) implementing 100 steps of genetic algorithm (Babel, 2011), while keeping all the default setting provided by Autodock Tools Visualization was done using Discovery studio (Tatar and Taskin Tok, 2019) and Chimera (Pettersen et al., 2004).

2.8. Molecular dynamics simulation

A molecular dynamics (MD) simulation study was done in an attempt to support the docking results. Following docking of ursolic acid in M3 protein and using cimetidine as the positive control drug (figure S4), GROMACS 2018 (Abraham et al., 2015) was used for the molecular dynamics simulation of the best pose. Chain A of the protein was simulated with maltose, tetraethylene glycole and the bound ligand, ursolic acid, in place of the co-crystallized ligand. Hydrogen atoms were added and the protein was prepared for simulations using Molecular Operating Environment (MOE) (Vilar et al.,
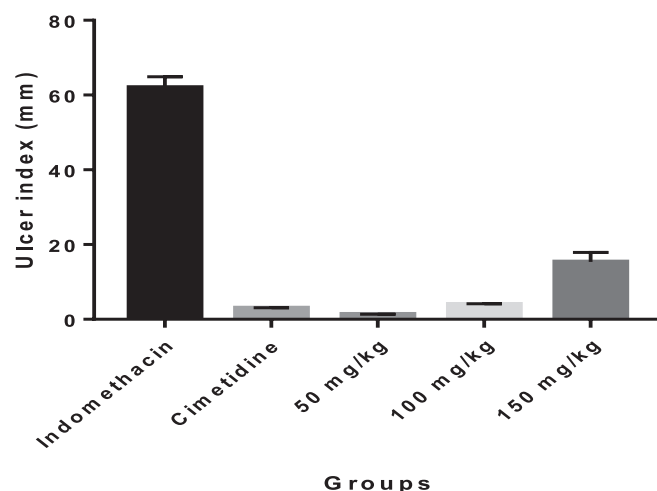

Fig. 4. Effect of different concentrations of UA on the ulcer index highlighting the concentration of 150 mg/kg as the highest one.

2008). For the molecular dynamics simulations, the forcefield AMBER99SB-ILDN was used for the protein while the GAFF force field was used for all the ligands (da Silva and Vranken, 2012). ACPYPE was used to facilitate ligand parameterization. The complex was then solvated in a dodecahedral water box which extends at least 1 nm in all directions. The TIP3P water model was used for solvation. The system was then neutralized by the addition of chloride ions. Extra sodium chloride was added to maintain a salt concentration of 150 mM. The system was minimized using the steepest descent algorithm, followed by 100 ps of NVT equilibration at 300 K, with position restraints on protein and ligands. Afterwards, NPT equilibration for 100 ps was performed under the same position restraints and at 1.0 bar pressure. All of the dynamics were performed with a short range cutoff of 1.2 nm for nonbonded interactions. Finally, position restraints were released and a 10-ns production phase was run, saving the coordinates every 10 ps. The trajectory was analyzed for RMSD equilibration and binding energy between urosolic acid and the receptor. The binding energy was estimated using the MM/PBSA method as implemented in the g_mmpbsa script developed by Baker et al. (2001) and Kumari et al. (2014). The estimation was performed
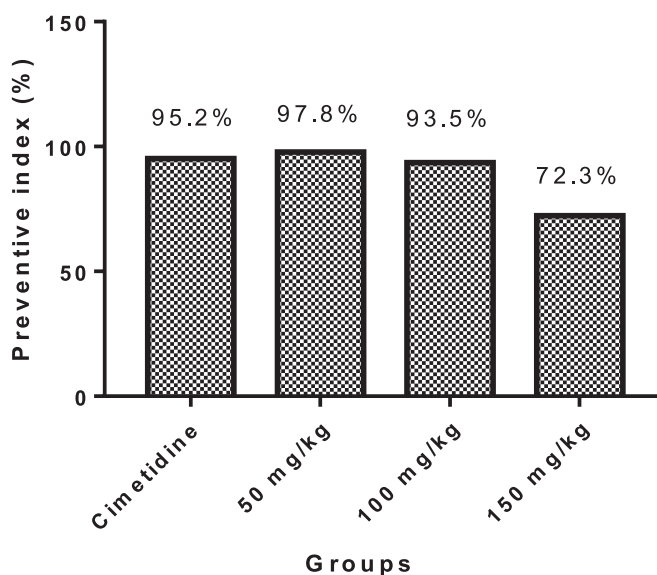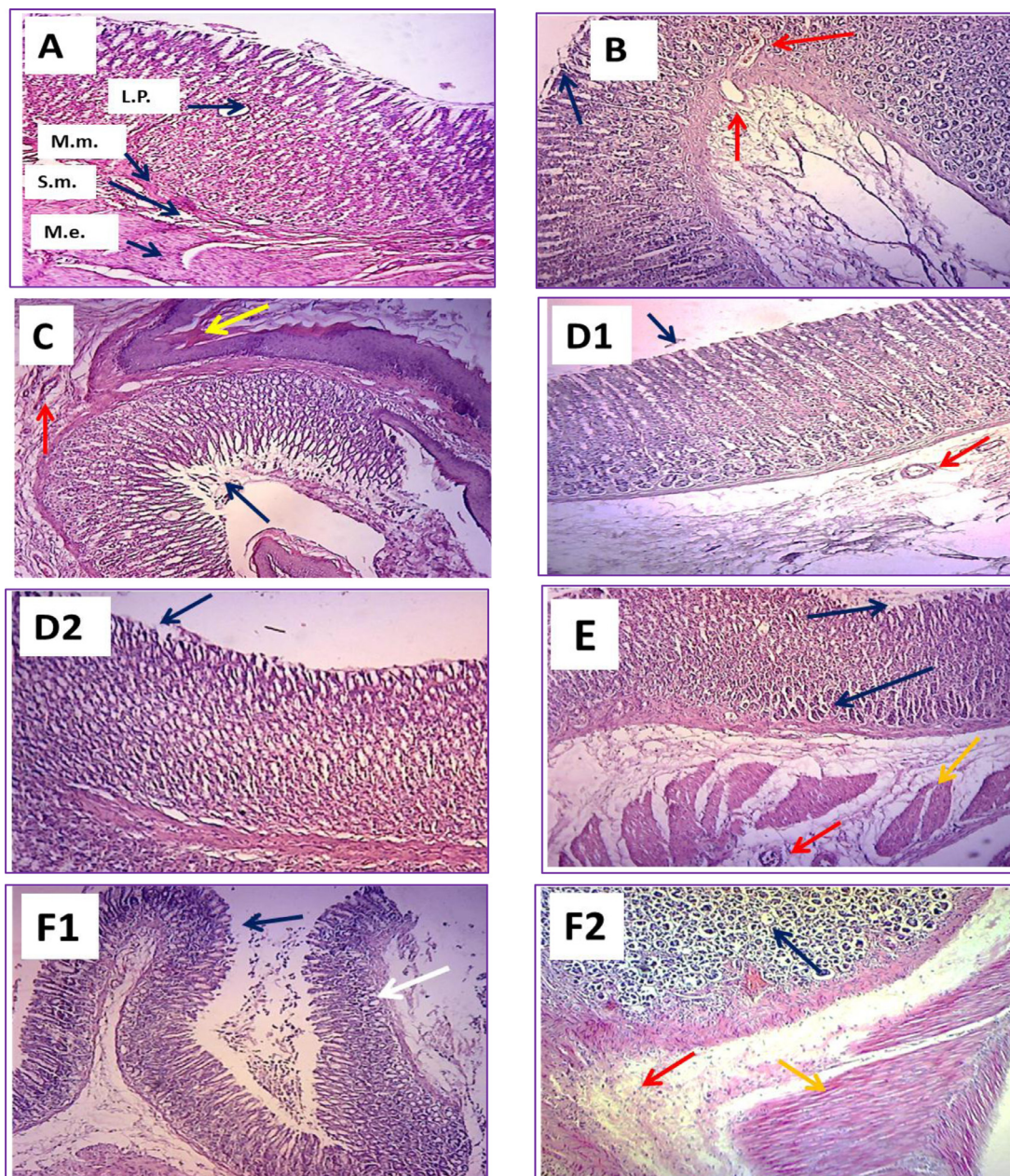

Fig. 5. Effect of different concentrations of UA on percentage inhibition of ulcer highlighting the concentration of 50 mg/kg as the highest one.

Fig. 6. (A-F2) LEM examination of sections from stomachs of rats from different groups. A (normal), B (+ve control), C (-ve control), D1, D2 (50 mg/kg UA), E (100 mg/kg UA), F1, F2 (150 mg/kg). (magnification 10 X).

on the last 8 ns of the simulation employing a solute dielectric constant of 2 and a solvent dielectric constant of 80. Default values were used for all other parameters of the calculation.

3. Results and discussion

In the present study, the Metabolic profiling of the DCM fraction from *O. forskolei* aerial parts was analysed and the antiulcer potential of ursolic acid was evaluated, since no attempt has been made earlier to construct such a study. The Metabolic profiling coupled with LC—HR-MS (Figure S1) revealed the presence of various classes of metabolites including: Triterpenes, diterpenes (mainly of abietane type), flavonoids, iridoids and caffeic acid derivatives and led to identification of 14 different metabolites using METLIN database. All of them were previously isolated from the genus *Ocimum*, and their

chemical structures are illustrated together with all their related data (Fig. 1and Table 1) (Figs. 2 and 3).

Chromatographic separation techniques using column chromatography led to precipitation of ursolic acid which was identified *via* ^{1}H NMR spectroscopic analysis (Figs. S2 A−C) as well as comparison with the authentic UA giving a R_f value of 0.77 and intense pinkish violet spot up on spraying with 1% vanillin-sulphuric acid reagent (Fig. S3).

The ADME toxicity analysis was predicted using the online platform of SwissADME (Daina et al., 2017). The summary of data is provided in Table S1 and it predicts the excellent oral bioavailability and the absence of CNS penetration of ursolic acid leading to the least possible side effects.

The docking results showed that ursolic acid has high docking scores with three proteins (−10.2, −10.2 and −11.8 Kcal/mol with
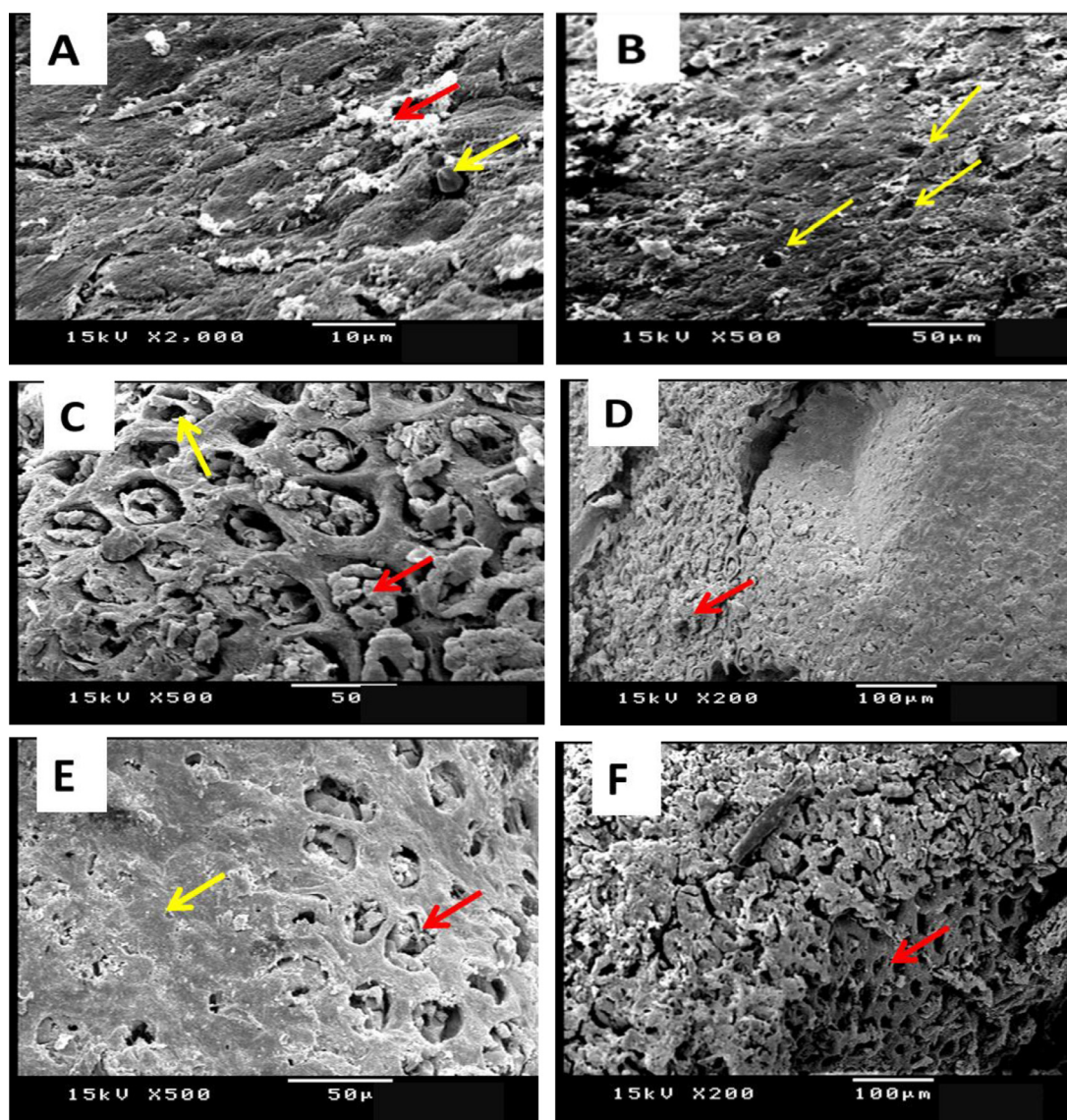
Fig. 7. (A-F) SEM examination of sections from stomachs of rats from different groups. A (normal), B (+ve control), C (-ve control), D (50 mg/kg UA), E (100 mg/kg UA), F (150 mg/kg).

CCK2, H2 and M3, respectively) as illustrated in Table S2. Its low docking score with the proton pump protein (−7.4 Kcal/mol) discourages considering its action to involve this pathway. Docking proglumide in the predicted active site of CCK2 resulted in H-bonds with the basic residues His376 and Arg356. Ursolic acid, on the other hand, fails to have similar interactions. H2-receptor blockers should possess a functional group to interact with a negatively charged ion in the active site (Ganellin, 1981). Docking of cimetidine in the homology model resulted in H-bonds with Asp 98 via the cyanoguanidine group and with Thr103 and Val99 via the sulfur atom. Similar to the case with CCK2, ursolic acid failed to reproduce the same behavior in docking. The predicted network of interaction with the active site of H2 is illustrated in Fig. 5.

For M3 receptor, the co-crystallized ligand interacts with Ser151 and Asn507 via H-bonds and forms π-stacking with Trp503 and Tyr529 as illustrated in Fig. 6. On the other hand, ursolic acid forms one H-bond and numerous van der Waals interactions in the active site. It can thus be concluded that the anti-ulcer activity of ursolic acid might involve interaction at the M3 receptor. This is further investigated via molecular dynamics.

The RMSD of both ligand and the protein alpha carbons were analyzed for the MD trajectory after fitting the alpha carbons to those of

the minimized structure. Figure S4 shows the change of RMSD over the course of the simulation time. As the figure shows, the protein is already equilibrated at a stable RMSD value around 0.4 nm early in the simulation. In addition, the ligand maintains an RMSD value of less than 0.2 nm in the binding pocket over most of the simulation time. This means that the ligand is stable in this binding pose that was present in the beginning of the simulation and continues to maintain the same binding pose until the end of the simulation. This suggests that the binding pose is stable and more likely to be the correct binding pose.

MM/PBSA calculations returned an estimated total binding energy of −344 kJ/mol between ursolic acid and the protein. The components of this binding energy come from −233 kJ/mol contribution from van der Waals interactions, −284 kJ/mol contribution from electrostatic interactions, 198 kJ/mol contribution from polar solvation energy and −24 kJ/mol contribution from non-polar solvation energy. Such a strong binding between ursolic acid and the M3 muscarinic acetylcholine receptor suggests that interaction with this receptor could be the mechanism through which ursolic acid achieves its anti-ulcer effect.

The antiulcer study of ursolic acid revealed its ability to inhibit the indomethacin-induced peptic ulcers in rats in a dose

dependent manner where group A (with the least dose of UA; 50 mg/kg) was the most protective one with UI 1.33 ± 0.33 and% inhibition 97.8 in comparison with cimetidine 3 ± 0.58 and 95.2%, where group B results were 4 ± 0.58 and 93.5% and group C gave the least protective results with 15.33 ± 3.18 and 72.3%, respectively (Table 2, Figs. 4 and 5).

Examining the opened stomachs of the indomethacin treated group (-ve control group) showed many ulcers of all levels, hyperaemia, heamorrhagic bands (yellow arrows) and petechial lesions (white arrows) (C1, C2). Tissues from group 3 (+ve control group) was the most protective one showing some ulcers of level 1 and mild hyperaemia. Those from group 4 showed a range of 1−2 ulcers of level 1 with no tissue hyperaemia, those from group 5 showed more ulcers of level 1 with hyperaemia while those from group 6 showed the least protection with ulcers of all levels, haemorrhagic lines and disruption to the surface mucosa (Figure S5).

LEM examination of Sections from group 1 (Fig. 6A) showed the normal architecture of the gastric tissue consisting of four layers: Lamina propria (L.P.), muscularis mucosa (M.m.), submucosa (S.m.) and Muscularis externa (M.e.). Those from group 2 (cimetidine group) showed some widening of gastric pits (blue arrows) with few congested blood vessels (red arrows) as well as edematous S.m. (white area) (Fig. 6B). Sections from group 3 (-ve control) showed deformation of gastric tissue, with wide areas of hemorrhage and thick mucous covering the surface (yellow arrows), necrosis to the M.m.(red arrows), deformation and widening of the gastric pits (blue arrows) and some congested blood vessels of the S.m. (Fig. 6C). Those from group 4 (50 mg/kg UA) showed the best results, some widening of gastric pits, rare congestions blood vessels and some or no edema of the S.m. (Fig. 6 D1 and D2). Tissues from group 5 (100 mg/kg UA) showed gastric pits widening, necrosis of the M.m., edema of S.m. and congestion of blood vessels as well as deep deformation of the M.e (Fig. 6E). Those from group 6 showed wider areas of damage, erosion of the surface, necrosis of the Muscularis mucosa (white arrow) and Muscularis externa (yellow arrow) as well as deep cellular infiltration of the S.m. (red arrows) (Fig. 6F).

SEM examination is employed to examine the surface mucosal and morphological changes occured to the gastric pits. The surface of normal tissues showed polygonal and dome-shaped gastric pits (yelow arrows) surrounded and lined by surface mucous cells with normal secretions of mucous (white arrows) (Fig. 7A). Examined tissues from group 2 showed nearly normal epithelium with some widened gastric pits (yellow arrows) as a result of epithelial destruction (Fig. 7B). Sections from group 3 showed many areas of ulceration penetrating deeply into mucosa. A complete shedding of surface mucous cells (superficial erosion) leaving the underlying gastric pit walls and openings with a honeycomb appearance. Remnants of the necrotic tissue are expressed with the red arrows while the yellow ones refer to widened openings of the gastric pits (Fig. 7C). Examining those from group 4 expressed nearly normal architecture of epithelial cells with few areas of superficial erosin leaving the gastric pits little widened and exposed (red arrows) (Fig. 7D). Areas of healthy intact epithelium (yellow arrows) interspersed by wide areas of surface erosion forming the honeycomb shape of gastric pits (red arrows) are shown clearly with tissues from group 5 (Fig. 7E). Those from group 6 showed wide areas of erosion as well as complete shedding of surface mucous cells and wide areas of tissue deformation (Fig. 7).

4. Conclusion

To the best of our knowledge, this is the first study to perform a Metabolic profiling and identification of various metabolites detected in the DCM fraction from *Ocimum forskolei*, the first time to evaluate the antiulcer potential of ursolic acid isolated from the same fraction with confirmation of its interaction with the relevant receptor proteins *via* molecular docking and molecular dynamic simulation analysis. The docking study showed that ursolic acid formed favorable interactions with M3 receptor with a binding score of −11.8, compared to cimetidine which showed no interaction with the receptor at all. MD study of the predicted binding pose showed a RMSD value of less than 0.2 nm which confirms the stability of the pose and supports the involvement of M3 receptor in the anti-ulcer mechanism of action of UA. It can be concluded from the above results that ursolic acid at a dose of 50 mg/kg, b.w. inhibited the indomethacin-induced ulcer in rats and provided the maximum protection of tissues which was clearly illustrated with LEM and SEM studies. The ADME-toxicity analysis showed excellent oral bioavailability with the absence of CNS penetration. The study could also establish the excellent antiulcer potential of the compound and provides a future tool for the dream of replacing synthetic drugs with natural and plant-origin ones with the maximum curative effects and the least possible side effects.

Declarations of Competing Interest

No potential conflict of interest was reported by the authors, and the procedurein compliance with the guidelines for the care and use of laboratory animals of the National Institutes of Health.

Supplementary materials

Supplementary material associated with this article can be found in the online version at doi:10.1016/j.sajb.2020.03.004.

References

Abraham, M.J., et al., 2015. GROMACS: high performance molecular simulations through multi-level parallelism from laptops to supercomputers. SoftwareX 1, 19–25.
Ali, N.A.A., et al., 2017. Antimicrobial, antioxidant, and cytotoxic activities of ocimum forskolei and teucrium yemense (Lamiaceae) essential oils. Medicines 4 (2), 1–14.
Arrieta, J., et al., 2003. Purification of gastroprotective triterpenoids from the stem bark of Amphipterygium adstringens; role of prostaglandins, sulfhydryls, nitric oxide and capsaicin-sensitive neurons. Planta Med. 69 (10), 905–909.
Arun, M., Asha, V., 2008. Gastroprotective effect of Dodonaea viscosa on various experimental ulcer models. J. Ethnopharmacol. 118 (3), 460–465.
Baba, M., et al., 2018. Molecular docking and quantitative structure-activity relationship study of anti-ulcer activity of quinazolinone derivatives. J. King Saud. Univ. Sci. 32 (2020), 657–666.
Babel, O., 2011. An open chemical toolbox O'Boyle Noel M; Banck Michael; James Craig A; Morley Chris; Vandermeersch Tim; Hutchison Geoffrey R. J. Cheminform. 3, 33.
Baker, N.A., et al., 2001. Electrostatics of nanosystems: application to microtubules and the ribosome. Proc. Natl. Acad. Sci. 98 (18), 10037–10041.
Baricevic, D., et al., 2001. Topical anti-inflammatory activity of Salvia officinalis L. leaves: the relevance of ursolic acid. J. Ethnopharmacol. 75 (2−3), 125–132.
Batista, L.M., et al., 2004. Gastric antiulcer activity of syngonanthus arthrotrichus silveira. Biol. Pharm. Bull. 27 (3), 328–332.
Cantrell, C.L., et al., 2001. Antimycobacterial plant terpenoids. Planta Med. 67 (08), 685–694.
Silva, Da, S., A.W., Vranken, W.F., 2012. ACPYPE-Antechamber python parser interface. BMC Res. Notes 5 (1), 1–8.
Daina, A., et al., 2017. SwissADME: a free web tool to evaluate pharmacokinetics, druglikeness and medicinal chemistry friendliness of small molecules. Sci. Rep. 7, 1–13.

Dekker, T., et al., 2011. Identification of mosquito repellent odours from Ocimum forskolei. Parasite Vector 4 (1), 1–7.

Elsayed, Y., et al., 2018. Metabolic profiling and biological investigation of the marine sponge−derived bacterium Rhodococcus sp. UA13. Phytochem. Anal. 29, 1–6.

Fatope, M.O., et al., 2008. Identification of the chemotypes of ocimum forskolei and ocimum basilicum by NMR spectroscopy. Chem. Biodivers. 5 (11), 2457–2463.

Ganellin, C., 1981. Medicinal chemistry and dynamic structure-activity analysis in discovery of drug acting at histamine H2 receptors. J. Med. Chem. 24, 913–920.

Giles, A.R., 1987. Guidelines for the use of animals in biomedical research. Thromb. Haemost. 58 (04), 1078–1084.

Inas, Z., et al., 2011. Gastroprotective effect of Cordia myxa L. fruit extract against indomethacin-induced gastric ulceration in rats. Life Sci. J. 8 (3), 433–445.

Kashiwada, Y., et al., 2000. Anti-AIDS agents 38. Anti-HIV activity of 3-O-acyl ursolic acid derivatives. J. Nat. Prod. 63 (12), 1619–1622.

Kim, E.S., Moon, A., 2015. Ursolic acid inhibits the invasive phenotype of SNU-484 human gastric cancer cells. Oncol. Lett. 9 (2), 897–902.

Kumari, R., et al., 2014. gammpbsa A Gromacs tool for high-throughput MM-PBSA calculations. J. Chem. Inf. Model. 54 (7), 1951–1962.

Lee, S.Y., et al., 2016. Recent studies on ursolic acid and its biological and pharmacological activity. EXCLI J. 15, 221–228.

Ma, J.Q., et al., 2015. Protective effects of ursolic acid in an experimental model of liver fibrosis through nRF2/are pathway. Clin. Res. Hepatol. Gastroenterol. 39 (2), 188–197.

Morris, G.M., et al., 2009. Autodock4 and autodocktools4: automated docking with selective receptor flexibility. J. Comput. Chem. 30 (16), 2785–2791.

Nanjundaiah, S.M., et al., 2011. Gastroprotective effect of ginger rhizome (Zingiber officinale) extract: role of gallic acid and cinnamic acid in H. Evid. Based Complement. Altern. Med. 1–13.

Ozbakiş, G.D., Gürsan, N., 2005. Effects of Momordica charantia L.(Cucurbitaceae) on indomethacin-induced ulcer model in rats. Turk. J. Gastroenterol. 16 (2), 85–88.

Pettersen, E.F., et al., 2004. UCSF chimera—a visualization system for exploratory research and analysis. J. Comput. Chem. 25 (13), 1605–1612.

Prabhu, K., et al., 2009. Ocimum gratissimum: a review of its chemical, pharmacological and ethnomedicinal properties. Open Complement. Med. J. 1, 1–15.

Schapoval, E.E., et al., 1998. Antiinflammatory and antinociceptive activities of extracts and isolated compounds from Stachytarpheta cayennensis. J. Ethnopharmacol. 60 (1), 53–59.

Singh, D., Chaudhuri, P.K., 2018. A review on phytochemical and pharmacological properties of Holy basil (Ocimum sanctum L.). Ind. Crop Prod. 118, 367–382.

Sumbul, S., et al., 2011. Role of phenolic compounds in peptic ulcer: an overview. J. Pharm. Bioallied Sci. 3 (3), 361–367.

Tatar, G., Taskin Tok, T., 2019. Structure prediction of eukaryotic elongation factor-2 kinase and identification of the binding mechanisms of its inhibitors: homology modeling, molecular docking and molecular dynamics simulation. J. Biomol. Struct. Dyn. 1–38.

Tawfike, A., et al., 2019. New bioactive metabolites from the elicited marine sponge-derived bacterium Actinokineospora spheciospongiae sp. nov. AMB Express 9 (1), 1–9.

Vilar, S., et al., 2008. Medicinal chemistry and the Molecular Operating Environment (MOE): application of QSAR and molecular docking to drug discovery. Curr. Top. Med. Chem. 8, 1555–1572.

Yang, Y., et al., 2015. Enhancement of radiation effects by ursolic acid in BGC-823 human adenocarcinoma gastric cancer cell line. PLoS One 10 (7), 1–9.